

Shadows and Strong Gravitational Lensing by Van der Waals Black Hole in Homogeneous Plasma

Niyaz Uddin Molla* and Ujjal Debnath†

Department of Mathematics, Indian Institute of Engineering Science
and Technology, Shibpur, Howrah-711103,India.

December 6, 2022

Abstract

In this paper, we first analyze the horizon structure of the Van der Waals(VdW) black hole and then investigate its shadow in the absence of a plasma medium as well as the presence of a homogeneous plasma medium. We find that both the Van der Waals parameters a and b have a significant effect on the shadow of the black hole. We also observe that the radius of the shadow in a homogeneous plasma medium decreases while parameter $\sigma = \frac{\omega_p}{\omega_\infty}$ (the ratio of plasma frequency and photon frequency) increases and the radius of the shadow inhomogeneous plasma medium is larger than the vacuum medium. We also discuss the strong gravitational lensing in a homogeneous plasma medium. We observe that the photon sphere radius, deflection limit coefficients and deflection angle in the strong field are highly affected by the presence of a homogeneous plasma medium. We also find that the deflection angle in the strong field limit by the Van der Waals black hole with the homogeneous plasma is greater than that of the Vacuum medium. Further, we discuss the observables quantities angular position θ_∞ , separation S and magnification r_{mag} by taking the example of a supermassive black hole in the strong field limit with the effects of homogeneous plasma. It is concluded that the Van der Waals parameters a , b and homogeneous plasma medium have a significant effect on both the shadows and strong gravitational lensing.

1 Introduction

One of the most powerful and important tools in astrophysics as well as cosmology is gravitational lensing(GL), which deals with the deflection light rays passing through the gravitational field. It has been successfully employed to explain for probing the strong characterization of gravity. Accordingly, the deflection angle of photon rays, the GL can be divided into scenarios, one of them is weak GL when the deflection angle is small, and another one is strong GL, when the deflection angle of photon rays becomes so larger. Strong GL was first investigated by darwin in 1959 [1] that the photons rays passing near to a black hole(BH) may have a large deflection angle and could make multiple loops around the BH before reaching to the observer. Leter, Virbhadra and Ellis [2], and Frittelli et al. [3] derived the exact lens equation regardless of background spacetime for arbitrary large value of deflection angle. After that Bozza et.al [4] developed an useful method to obtain the deflection angle of light rays by a compact object in the strong field limit, and they found the logarithmic divergence of the deflection angle for Schwarzschild BH in the strong field region. Later, Bozza et al. [5] extended the previous analysis for any general static, asymptotically spherically symmetric spacetime. In the last decades, strong GL regained more attention. [6–11].

In 2019, the first image of M87* was observed by the Event horizon Telescope (EHT) [11–16], which gives us the deeper understanding of BH physics and testing the various types of black BHs. One of the most important features of this image is that the event horizon of the BH is surrounded by a dark region called BH shadow and a bright-light ring encircled around the BH shadow. It is also known from some literature [17, 18, 26, 35] that the BH shadow is created by the BH effect. The study of BH shadow has been investigated by many authors for the different spacetimes [19–49].

*e-mail: niyazuddin182@gmail.com

†e-mail: ujjaldebnath@gmail.com

The BH as a thermodynamic system which is almost equivalent to the classical thermodynamic system. For the BH in Ads spacetime, the Ads charged BH is almost equivalent to the Van der Waals (VdW) fluid system. The BH is not only treated as a thermodynamic system, but it's also can be treated as a gravitational system in our universe.

The thermodynamic properties of the BH have an important role in the quantum gravity theory. Due to the Ads /CFT corresponds, the physics of asymptotically Ads BH great attention in the last decades. In the point of view of extended phase space [50, 51] where the cosmological constant ($\Lambda < 0$) is behave as a thermodynamic pressure p [52, 53]

$$p_\Lambda = -\frac{\Lambda}{8\pi} = \frac{3}{8\pi l^2} \quad (1)$$

is allowed to vary in the first law of thermodynamic

$$\delta M = T\delta S + V\delta p + \dots \quad (2)$$

where the thermodynamic volume V , thermodynamically conjugate to p is given by

$$V = \frac{\partial M}{\partial T} \Big|_{S, \dots} \quad (3)$$

Here M , S , T are the mass, entropy, temperature of the BH respectively.

In [54] Rajagopal et al. have shown asymptotically BH metric whose thermodynamic matches exactly with the Van der Waals (VdW) BH. The VdW fluid described by the closed form two parameter equation of state:

$$T = \left(p + \frac{a}{v^2}\right)(v - b) \quad (4)$$

Here, the specific volume of the VdW fluid is given by $v = \frac{V}{N}$, Where N is the degrees of freedom of the fluid and V is the volume occupied by the fluid. The constant $a > 0$ measures the intermolecular forces in the fluid and the constant $b > 0$ measures the volume of the molecules.

In recent years, Van der Waals BH has been investigated in various astronomical aspects such as, BHs as heat Engine [55]. In this work, we discussed the shadow and strong GL with the effects of homogeneous plasma.

A Plasma is a dispersive medium, and when light rays pass through the dispersive medium, they are refracted by this medium before reaching to the observer. From an astrophysical point of view, all photons mostly go through a plasma medium. On the other hand, the plasma medium can affect the angular position of an equivalent image, giving various wavelengths in observation.

This is the most intriguing and important reason why one needs to consider the plasma medium in the analysis of GL. To calculate the deflection angle of the photon rays and shadows of the BH in the presence of plasma and gravity, we apply the method [56, 57] which has been discussed in detail in the books (see [58, 59]).

The effect of plasma on the shadow of BHs and wormholes have been widely investigated by some authors [60–64]. GL by the BH in a homogeneous plasma, the medium was studied in [65–73].

The paper is arranged as follows: In Sec.2, we review the VdW spacetime and the null geodesics equation. In Sec.3, we study the shadows of the VdW BH in the absence of a plasma medium. In Sec.4, We study the shadows of the Van der Waals BH with the presence of plasma medium. We discuss the strong GL of Van der Waals BH with the effects of homogeneous plasma medium in Sec.5. Further, we also discuss the strong observable quantity in Sec.6. Finally, we discuss and conclude the study in Sec.7.

2 Van der Waals spacetime and Null geodesic equations

We start with a spherically symmetric, static Ads spacetime, constructed by Rajagopal [54] as

$$ds^2 = -f(r)dt^2 + \frac{dr^2}{f(r)} + r^2 d\theta^2 + r^2 \sin^2 \theta d\phi^2 \quad (5)$$

where

$$f(r) = 2\pi a - \frac{2M}{r} + \frac{r^2}{l^2} \left(1 + \frac{3b}{2r}\right) - \frac{3\pi ab^2}{r(2r + 3b)} - \frac{4\pi ab}{r} \log\left(\frac{r}{b} + \frac{3}{2}\right) \quad (6)$$

The event horizon of the BH locates at $r = r_+$. The horizon radius r_+ is determinants by the solutions of the equation $f(r_+) = 0$ i.e.,

$$2\pi a - \frac{2M}{r_+} + \frac{r_+^2}{l^2} \left(1 + \frac{3b}{2r_+}\right) - \frac{3\pi ab^2}{r_+(2r_+ + 3b)} - \frac{4\pi ab}{r_+} \log\left(\frac{r_+}{b} + \frac{3}{2}\right) = 0 \quad (7)$$

whose real roots are shown graphically in Fig.1 and Table.1

It has been shown that the spacetime solution (5) does not satisfied any of the standard energy conditions everywhere out sides the horizon but for the sufficiently small pressure p , energy condition can be satisfied in the neighbouring of the BH horizon. The Lagrangian represents the motion of light rays around the spacetime (5) is given by

$$2\mathcal{L} = -f(r)\dot{t}^2 + (f(r))^{-1}\dot{r}^2 + r^2\dot{\theta}^2 + r^2\sin^2\theta\dot{\phi}^2 \quad (8)$$

which is used to calculate the geodesic equations. Here dot indicates the derivative w.r.t the affine parameter. The null geodesic equations for photon motion are given by

$$\dot{t} = \frac{E}{f(r)} \quad (9)$$

$$r^2\dot{\theta} = \pm\sqrt{\Theta} \quad (10)$$

$$\dot{\phi} = \frac{L}{r^2\sin^2\theta} \quad (11)$$

$$r^2\dot{r} = \pm\sqrt{\mathcal{R}} \quad (12)$$

where

$$\Theta = K - \frac{L^2}{\tan^2\theta}$$

$$\mathcal{R} = E^2r^4 - r^2(L^2 + k)f(r)$$

and L, E are the angular momentum and Energy of the photon respectively. From the equation (10), one can write the equation as

$$\dot{r}^2 + V_{eff} = 0 \quad (13)$$

where V_{eff} is the effective potential function and it is obtained by

$$V_{eff} = \frac{f(r)}{r^2}(K + L^2) - E^2$$

Now, we change the effective potential function V_{eff} with respect to the new impact parameters such as $\xi = \frac{L}{E}$ and $\eta = \frac{K}{E^2}$

$$V'_{eff} = \frac{E^2}{r^2}\{(\eta + \xi^2)f(r) - r^2\} \quad (14)$$

Table 1: The horizon radius for the different values of the parameters a and b .

| a | b | r_+ |
|-----|-----|-----------|
| 0.1 | 0.2 | 0.019247 |
| | 0.4 | 0.014729 |
| | 0.6 | 0.0128272 |
| | 0.8 | 0.0117176 |
| 0.3 | 0.2 | 0.02165 |
| | 0.4 | 0.0179965 |
| | 0.6 | 0.0165162 |
| | 0.8 | 0.0156372 |
| 0.5 | 0.2 | 0.023765 |
| | 0.4 | 0.020694 |
| | 0.6 | 0.019423 |
| | 0.8 | 0.0187867 |
| 0.7 | 0.2 | 0.025927 |
| | 0.4 | 0.023051 |
| | 0.6 | 0.022055 |
| | 0.8 | 0.021392 |

From the Fig.1 and Table.1, we can see that for the fixed value of the parameter a , the horizon radius r_+ decreases by the increasing value of parameter b but for the fixed value of the parameter b , the horizon r_+ increases by the increasing value of parameter a .

3 Shadow of Van der Waals black hole

In this section, we study the shadow of Van der Waals BH with the absence of plasma medium.

In order to describe the boundary of the unstable photon circular orbit, one has to satisfies the effective potential critical conditions

$$V_{eff} = 0 = \frac{\partial V_{eff}}{\partial r} \Big|_{r_0}, \frac{\partial^2 V_{eff}}{\partial r^2} \Big|_{r_0} > 0 \quad (15)$$

Using (14) and solving the equation (15), we obtain the equation of unstable photon circular orbit in the form

$$\frac{f'(r)}{f(r)} = \frac{2}{r} \quad (16)$$

The Photon sphere radius r_c can be obtained graphically, from the function

$$F(r) = r f' - 2f(r) = 0 \quad (17)$$

Table 2: Estimation of radius of the photon sphere and the radius of the shadows for the different values of the parameter a and b .

| a | b | r_c | r_s |
|-----|-----|---------|----------|
| 0.1 | 0.2 | 0.07215 | 0.018129 |
| | 0.4 | 0.05146 | 0.012494 |
| | 0.6 | 0.04255 | 0.010087 |
| | 0.8 | 0.03745 | 0.008743 |
| 0.3 | 0.2 | 0.07419 | 0.018315 |
| | 0.4 | 0.05460 | 0.012746 |
| | 0.6 | 0.04639 | 0.010347 |
| | 0.8 | 0.04137 | 0.008921 |
| 0.5 | 0.2 | 0.07650 | 0.018774 |
| | 0.4 | 0.05762 | 0.013340 |
| | 0.6 | 0.05046 | 0.011093 |
| | 0.8 | 0.04525 | 0.009629 |
| 0.7 | 0.2 | 0.07844 | 0.019163 |
| | 0.4 | 0.06051 | 0.013897 |
| | 0.6 | 0.05344 | 0.011653 |
| | 0.8 | 0.04965 | 0.010373 |

The radius of Shadow r_s at the Photon sphere radius r_c is given by

$$r_s = \sqrt{\xi^2 + \eta} = \frac{r_c}{\sqrt{f(r_c)}} \quad (18)$$

The shadow boundary curve of the BH at the celestial co-ordinate (α, β) define as

$$\alpha = \lim_{r_0 \rightarrow \infty} (r_0^2 \sin \theta_0) \frac{d\phi}{dr} \quad (19)$$

$$\beta = \lim_{r_0 \rightarrow \infty} (r_0^2 \frac{d\theta}{dr}) \quad (20)$$

where r_0 is the radial distance of the BH with respect to the observer and θ_0 is the inclination angle between the BH and observer. With the help of the equations ((10),(11)and (12) and doing some simplification, one can obtain the celestial co-ordinates as

$$\alpha = -\frac{\xi}{\sin \theta_0}, \quad (21)$$

$$\beta = \sqrt{\eta - \frac{\xi^2}{\tan^2 \theta_0}} \quad (22)$$

Simplifying the equations (21) and (22),we obtain the following equation

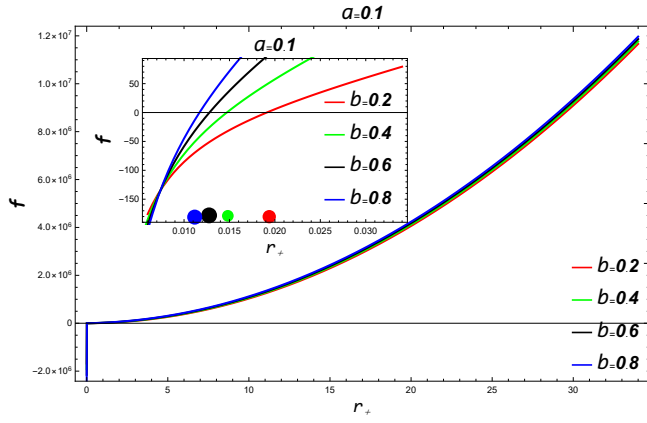
$$\alpha^2 + \beta^2 = \xi^2 + \eta \quad (23)$$

Using the equations (18) and 23), we construct the shape of the VdW BH shadow. We plot the shadow shape with α versus β for the different values of the parameters a and b in Fig.3. From Fig.3 and Table.2, we can see that for the fixed value of the parameter a , the photon sphere radius r_c and the radius of the shadow of BH r_s is decreased by increasing the value of parameter b but for the fixed value of the parameter b , the photon sphere radius r_c and the radius of the shadow of BH r_s is increased by increasing the value of parameter a .

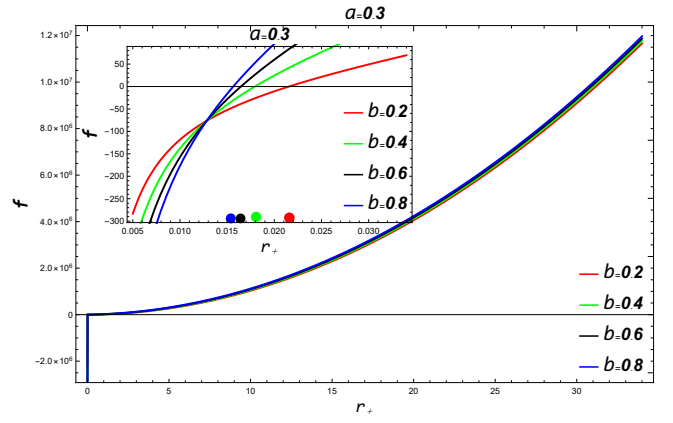
4 Effect of homogeneous Plasma on Shadow of Van der Waals black hole

In this section, we investigate the Van der Waals BH shadow in the presence of homogeneous plasma medium. So, We consider that the spacetime is filled with a homogeneous plasma . If we denote the mass and the charge of the electron m and e respectively, then the electron plasma frequency is given by

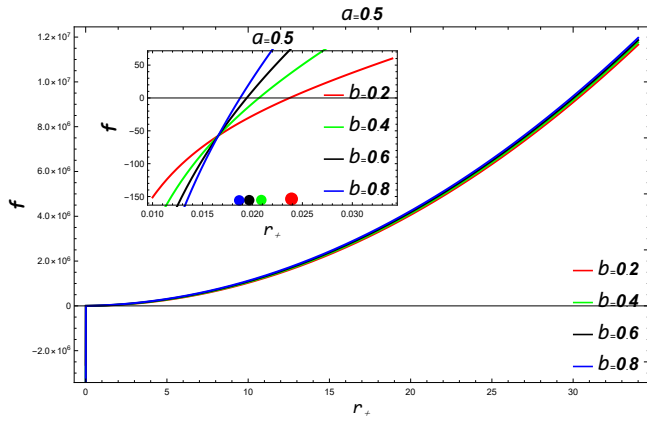
$$\omega_p(r)^2 = \frac{4\pi e^2}{m} N(r) \quad (24)$$



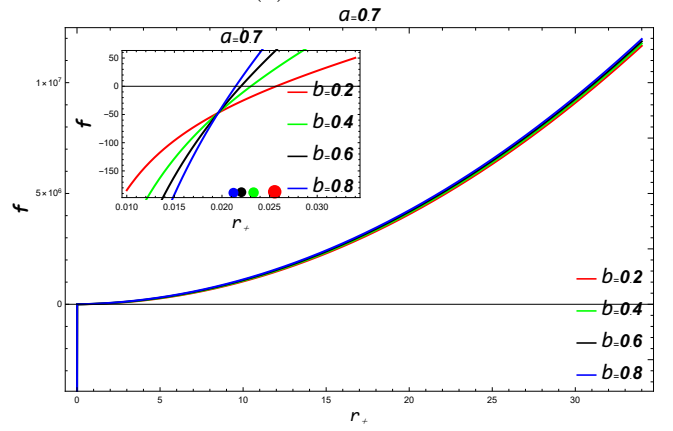
(a)



(b)



(c)



(d)

Figure 1: The BH horizon, where the horizontal axis denoted by r_+ and vertical axis by f . The pictures for $a = 0.1, a = 0.3, a = 0.5$ and $a = 0.7$ for the different values of $b = 0.2, b = 0.4, b = 0.6, b = 0.8$.

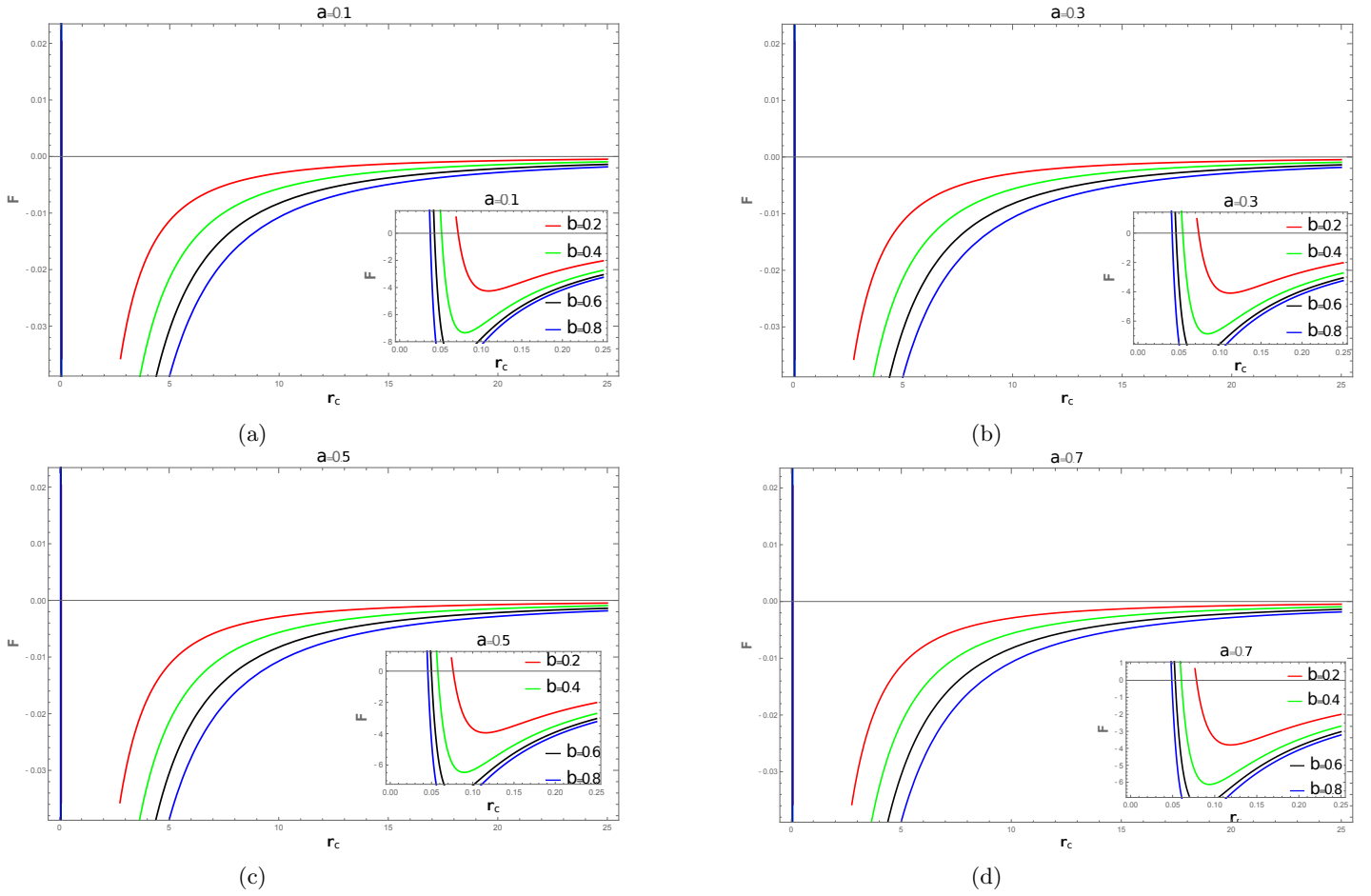


Figure 2: The photon sphere radius r_c , where the horizontal axis denoted by r_c and the vertical axis by F . The pictures for $a = 0.1, a = 0.3, a = 0.5$ and $a = 0.7$ for the different values of $b = 0.2, b = 0.4, b = 0.6, b = 0.8$.

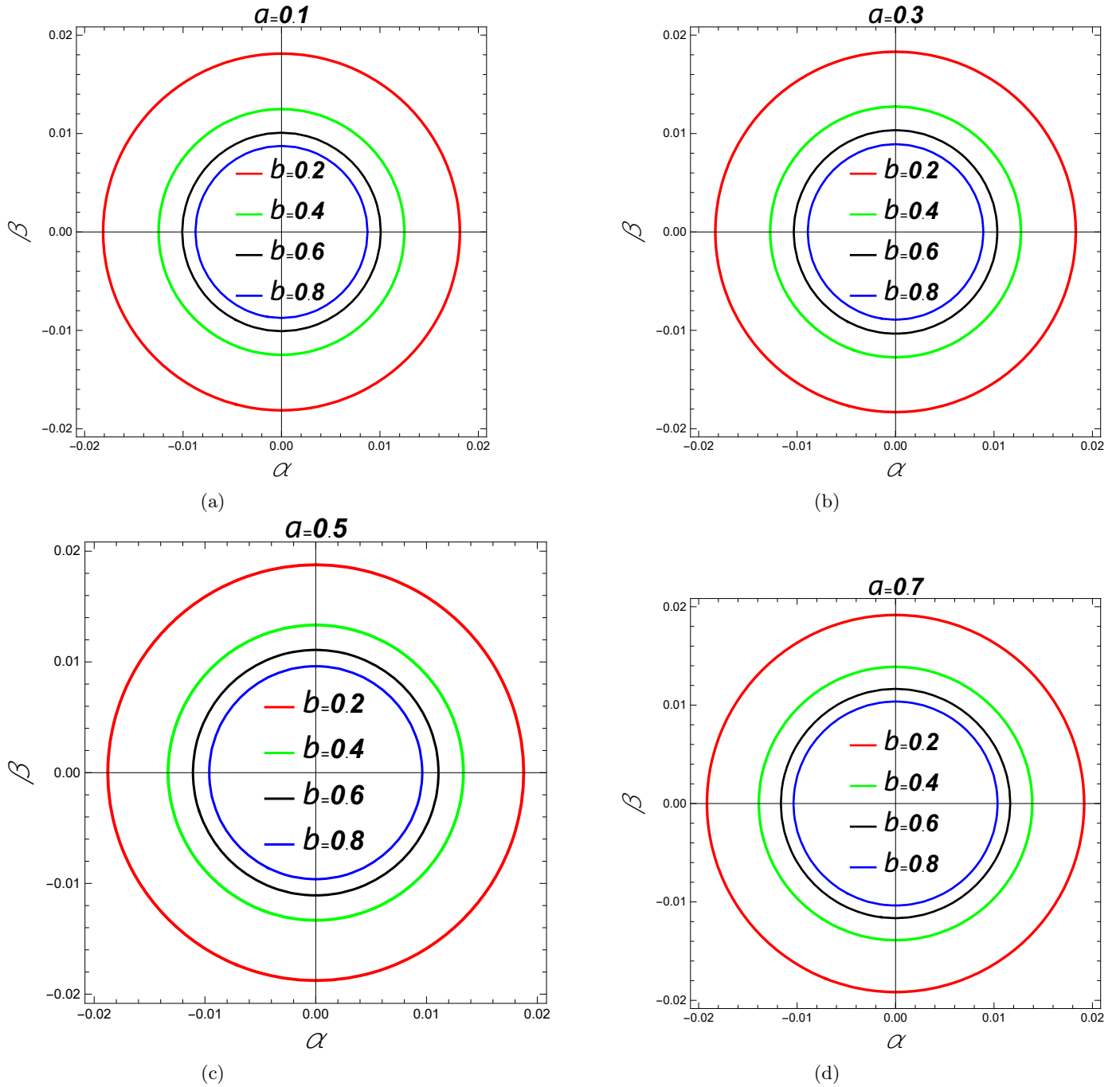


Figure 3: The BH shadows in the absence of plasma medium, where the horizontal axis denoted by r_c and the vertical axis by F . The pictures for $a = 0.1, a = 0.3, a = 0.5$ and $a = 0.7$ for the different values of $b = 0.2, b = 0.4, b = 0.6, b = 0.8$.

where electron number density $N(r)$ as a function of radius coordinates only. The refraction index n is related to the photon frequency, reads as

$$n^2 = 1 - \frac{\omega_p(r)^2}{\omega_\infty^2} = 1 - \sigma^2 \quad (25)$$

where parameter $\sigma = \frac{\omega_p}{\omega_\infty}$ represents the ratio of plasma frequency and photon frequency.

It is observe that the photon can propagate through the plasma if $\omega_p < \omega_\infty$ and the photon motion is forbidden while $\omega_p > \omega_\infty$. It is clear that the value $n = 1$ is in the vacuum case.

It is useful to define the function [78]

$$h(r)^2 = r^2 \left(\frac{1}{f(r)} - \frac{\omega_p^2}{\omega_\infty^2} \right) \quad (26)$$

With the help of the above equation, one can calculate radius of the photon sphere r_c as real roots of the equation

$$\frac{d}{dr}(h(r)^2) = 0 \quad (27)$$

$$H(r) = \frac{2r}{f(r)} - r^2 \frac{f'(r)}{(f(r))^2} - 2r \frac{\omega_p^2}{\omega_\infty^2} = 0 \quad (28)$$

The angular radius of the Shadow is defined as follows

$$\sin^2(\alpha_s) = \frac{r_c^2 \left(\frac{1}{f(r_s)} - \frac{\omega_p^2}{\omega_\infty^2} \right)}{r_o^2 \left(\frac{1}{f(r_o)} - \frac{\omega_p^2}{\omega_\infty^2} \right)} \quad (29)$$

For the Vacuum case, $\omega_p = 0$

$$\sin^2(\alpha_s) = \frac{r_c^2}{r_o^2} \frac{f(r_s)}{f(r_o)} \quad (30)$$

where r_c is given from the equation (26) graphically.

Solving the equation (28), we graphically obtain the radius of the photon sphere in the presence of plasma medium and using this radius, we construct the shape of shadows of the BH in a homogeneous plasma medium. We plot the shadow shape with α versus β in Fig.5. We can see from Fig.5 and Table.3 that the radius of the shadow of the BH decreases by increasing the value of parameter σ , and we also noticed that the radius of the BH shadow in the presence of plasma is bigger than the vacuum one.

Table 3: Estimation of the photon sphere radius r_c and the shadow radius of the black hole r_s for the different values of the parameter σ .

| $\sigma = \frac{\sigma_p}{\sigma_\infty}$ | $0 < r_c < 1$ | r_s | $\sigma = \frac{\sigma_p}{\sigma_\infty}$ | $1 < r_c < \infty$ | r_s |
|---|---------------|-----------|---|--------------------|------------|
| 0.000 | 0.078516 | 0.0139318 | 0.001 | 3.54159 | 0.09978958 |
| 0.001 | 0.078704 | 0.0160289 | 0.002 | 1.63751 | 0.09954998 |
| 0.002 | 0.079342 | 0.0153975 | 0.003 | 1.00143 | 0.09927789 |
| 0.003 | 0.080528 | 0.0145246 | | | |

Using the equation (29) and Table.3, we obtain the angular size of the shadow of the BH and the variation of its displayed in Fig.6. In this figure, we see that the angular size of shadow is decreased with the position of a static observer r_o for the different value of the parameter $\sigma = \frac{\omega_p}{\omega_\infty}$.

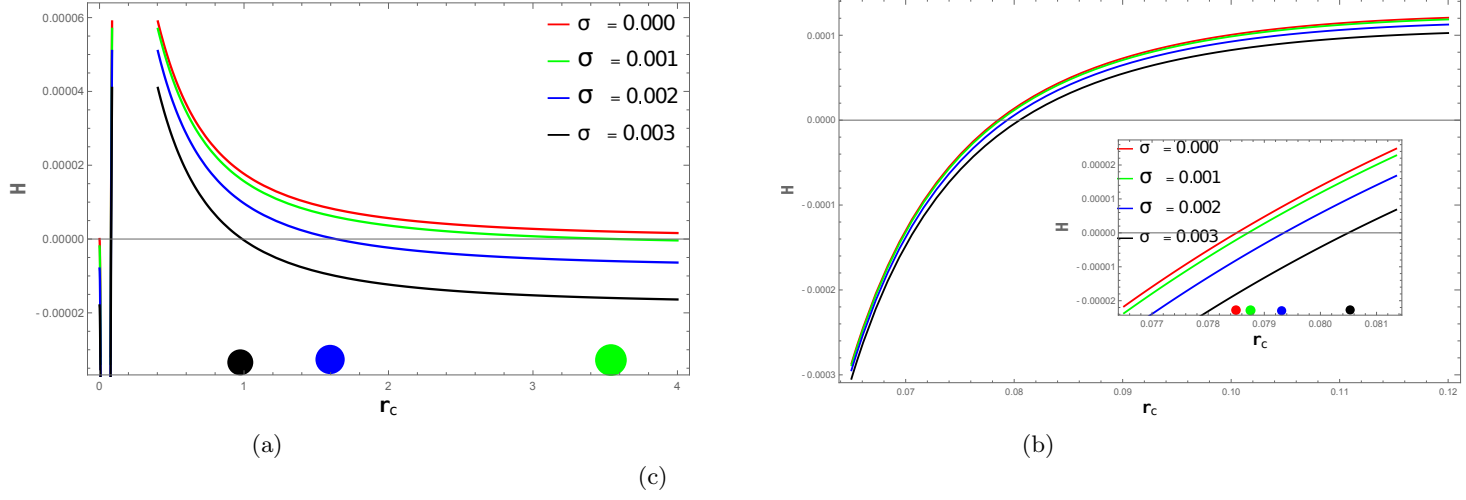


Figure 4: The photon sphere radius r_c , where the horizontal axis denoted by r_c and the vertical axis by H . Right panel for the case photon sphere radius r_c within the range $0 < r_c < 1$ and Left panel for the case photon sphere radius $r_c \geq 1$.

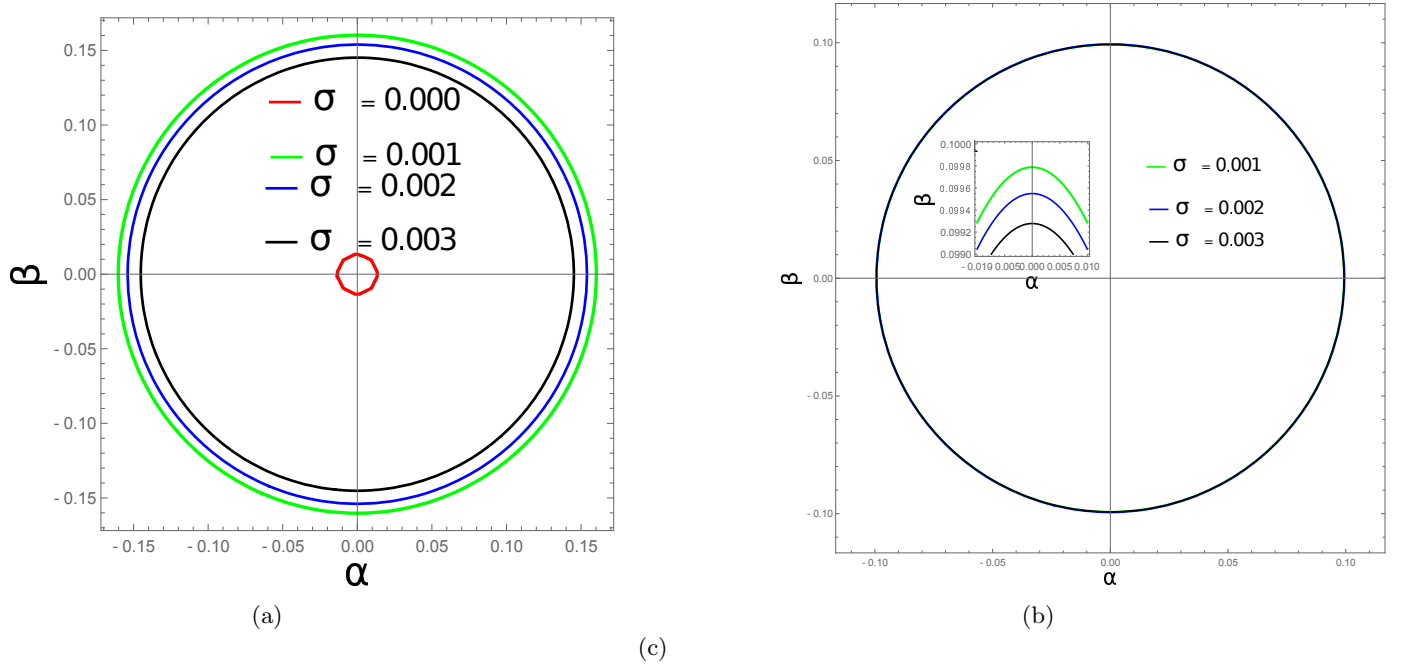


Figure 5: The black hole shadows in the presence of different plasma medium ($\sigma = 0.000, 0.001, 0.002, 0.003$), where the horizontal axis denoted by α and the vertical axis by β . Parameter $\sigma = \frac{\omega_p}{\omega_{\infty}}$ represents the ratio of plasma frequency to the photon frequency. Left panel for the case photon sphere radius r_c within the range $0 < r_c < 1$ and Right panel for the case photon sphere radius $r_c > 1$. In the Left panel, the red circle represents the shadow shape in vacuum medium.

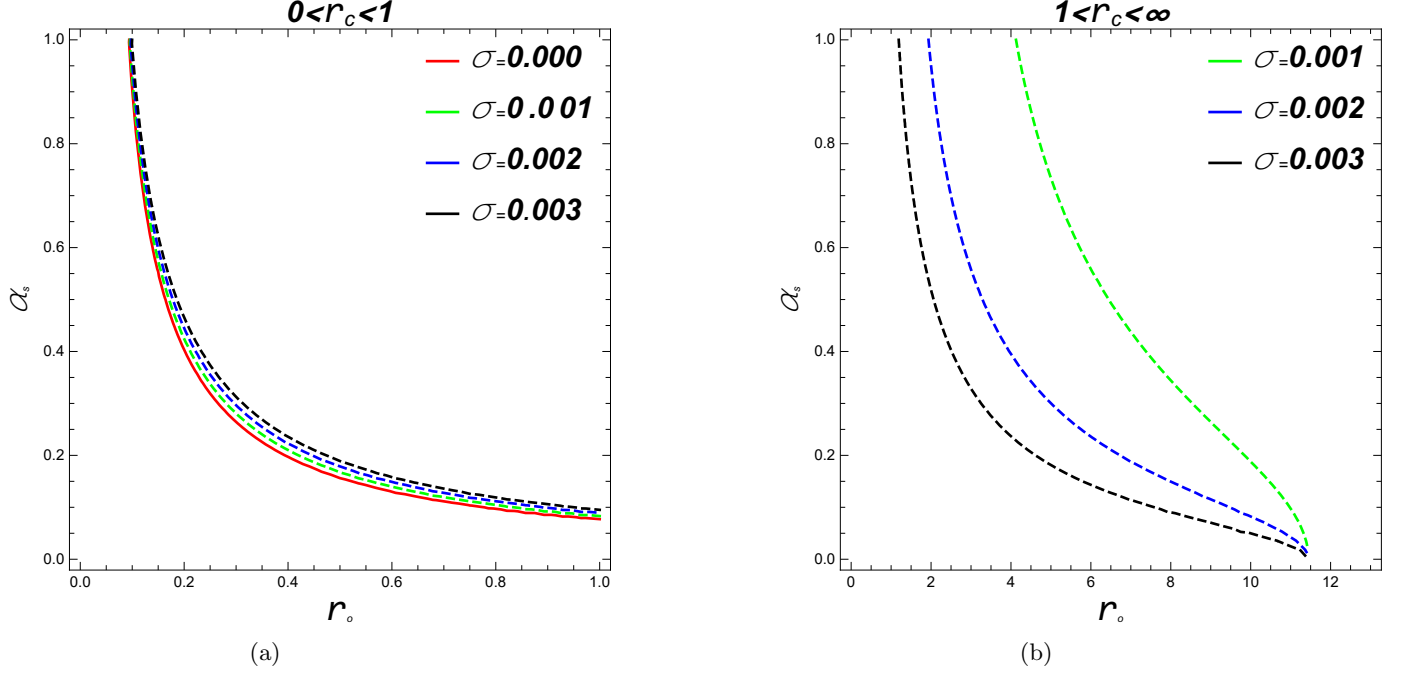


Figure 6: Behaviour of angular size of the shadow of BH with respect to the position of a static observer r_o with different value of $\sigma = 0.000, 0.001, 0.002, 0.003$. Left panel represents the angular size of shadow when the photon sphere radius $r_c < 1$ and right panel represents the angular size of shadow when the photon sphere radius $r_c > 1$. Parameter $\sigma = \frac{\omega_p}{\omega_\infty}$ represents the ratio of plasma frequency and photon frequency.

5 Strong gravitational lensing with the effects of homogeneous plasma

In this section we discuss the strong GL on the equatorial plane ($\theta = \frac{\pi}{2}$) in the presence of homogeneous plasma. The metric (5) can be written on the equatorial plane ($\theta = \frac{\pi}{2}$) as

$$ds^2 = -F(r)dt^2 + G(r)dr^2 + K(r)d\phi^2 \quad (31)$$

where

$$F(r) = f(r) = 2\pi a - \frac{2M}{r} + \frac{r^2}{l^2} \left(1 + \frac{3b}{2r}\right) - \frac{3\pi ab^2}{r(2r+3b)} - \frac{4\pi ab}{r} \log\left(\frac{r}{b} + \frac{3}{2}\right) \quad (32)$$

$$G(r) = (f(r))^{-1} = \left\{2\pi a - \frac{2M}{r} + \frac{r^2}{l^2} \left(1 + \frac{3b}{2r}\right) - \frac{3\pi ab^2}{r(2r+3b)} - \frac{4\pi ab}{r} \log\left(\frac{r}{b} + \frac{3}{2}\right)\right\}^{-1} \quad (33)$$

and

$$K(r) = r^2 \quad (34)$$

The Hamiltonian for the light rays around the Van der Waals BH when it's surrounded by plasma can be expressed as in Ref. [74]

$$H(x^i, p_i) = \frac{1}{2} [g^{ik} P_i P_k + w_p^2] \quad (35)$$

where g^{ik} is the contravariant tensor of the metric (31) and P_i is the momentum of photon.

Here, we consider the homogeneous plasma with $\omega_p = \text{constant}$. Using the equation (35), we can obtain the Hamiltonian differential equations for the photon around the black hole as

$$\frac{dx^i}{d\lambda} = \frac{\partial H}{\partial p_i}, \quad \frac{dx^i}{d\lambda} = -\frac{\partial H}{\partial x^i} \quad (36)$$

and hence, we obtain two constants of motions which are the angular momentum L and the energy E of the photon

$$L = P_\phi, E = -p_t = \omega_\infty, \quad (37)$$

where ω_∞ is the frequency of photon coming from infinity.

Using the Eqs. (31) and (36), the expression for $dr/d\lambda, d\phi/d\lambda$ can be written as

$$\frac{dr}{d\lambda} = \frac{\partial H}{\partial p_r} = \frac{p_r}{G(r)} \quad (38)$$

$$\frac{d\phi}{d\lambda} = \frac{\partial H}{\partial x^i} = \frac{p_\phi}{K(r)} \quad (39)$$

Using the Eqs (38) and (39), one can find the equation of photon trajectory as in Ref. [75, 76]

$$\left(\frac{dr}{d\phi}\right)^2 = \frac{R_p(r)K(r)}{G(r)} \quad (40)$$

Where

$$R_p = \frac{E^2 K(r) W(r)}{L^2 F(r)} - 1 \quad (41)$$

and

$$W(r) = 1 - \frac{\omega_p^2(r)F(r)}{E^2} = 1 - \frac{\omega_p^2(r)}{\omega_\infty^2} F(r) = 1 - \sigma^2 F(r) \quad (42)$$

where parameter $\sigma = \frac{\omega_p}{\omega_\infty}$ represents the ratio of plasma frequency and photon frequency.

In particular, $\omega_p(r) = 0$ as well as $W(r) = 1$, in the Eq. (42) represent the motion of photon ray in vacuum medium.

As the photon rays coming from infinity and reaches to closest distance $r = r_0$ and then goes out to infinity. So, for the minimum distance of photon trajectory, $\frac{dr}{d\phi}$ vanishes and hence, we have the minimum impact parameter as [77]

$$u(r_0) = \frac{L}{E} = \frac{K(r_0)}{F(r_0)} \frac{\dot{\phi}}{\dot{t}} = \sqrt{\frac{K(r_0)W(r_0)}{F(r_0)}} \quad (43)$$

To find the photon sphere radius for the unstable circular orbit of photon for static, spherically symmetric BH, we consider a function $h(r)$ given by ref. [78] as

$$(h(r))^2 = \frac{W(r)K(r)}{F(r)} = \frac{K(r)}{F(r)} \left\{1 - \frac{\omega_p^2 F(r)}{E^2}\right\} \quad (44)$$

The photon sphere radius r_c is the largest real root of the following equation

$$\frac{d}{dr} \{(h(r))^2\} = 0 \quad (45)$$

Simplifying the equations (44) and (45), we obtain,

$$\frac{K'}{K} + \frac{W'}{W} - \frac{F'}{F} = 0 \quad (46)$$

where \prime denotes the differentiation with respect to r .

One can solve the equation (46), we obtain the photon sphere radius r_c and its behaviour is shown in Fig.7. The photon sphere radius r_c increases with the parameter a (left panel) as well as the parameter b (right panel) in Fig.7. We can see that The photon sphere radius r_c in a homogeneous plasma medium is greater than the vacuum one.

We define minimum impact parameter u_c at $r_0 = r_c$, for the light ray as

$$u(r_c) = \sqrt{\frac{K(r_c)W(r_c)}{F(r_c)}} \quad (47)$$

which is shown in Fig.8. In this figure, we can see that for the fixed value of the parameter σ , the minimum impact parameter u_c decreases with the parameter a (left panel) and increases the parameter b (right panel).

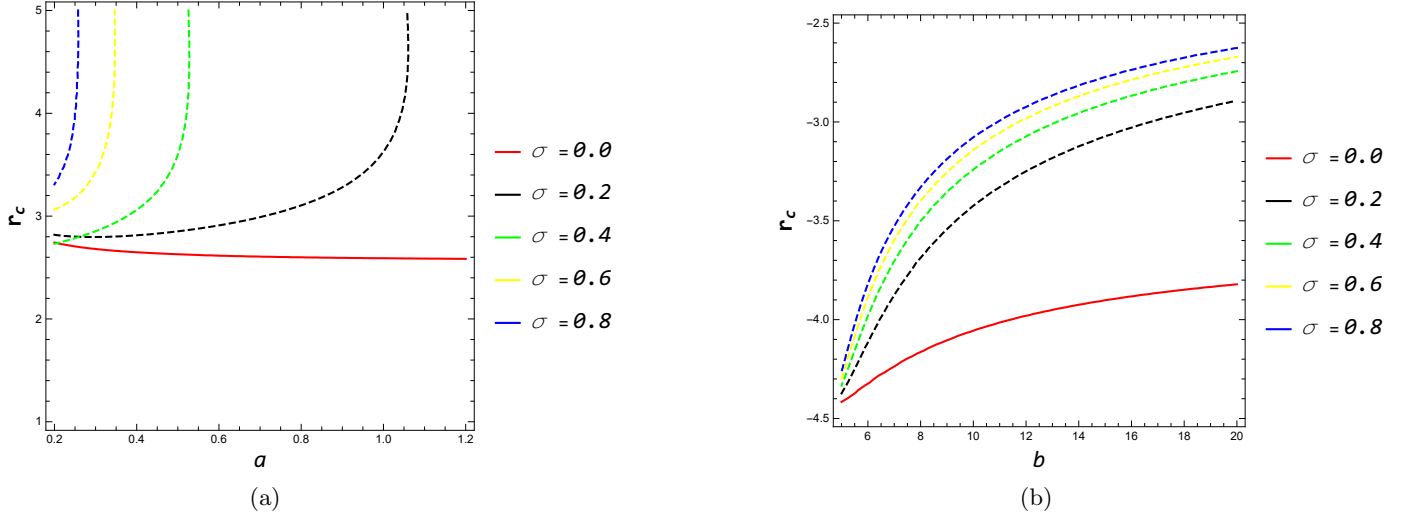


Figure 7: The radius r_c as a function of a (Left panel) and b (Right panel) for the values of $\sigma = 0.0, 0.2, 0.4, 0.4, 0.6, 0.8$. Parameter $\sigma = \frac{\omega_p}{\omega_\infty}$ represents the ratio of plasma frequency to the photon frequency.

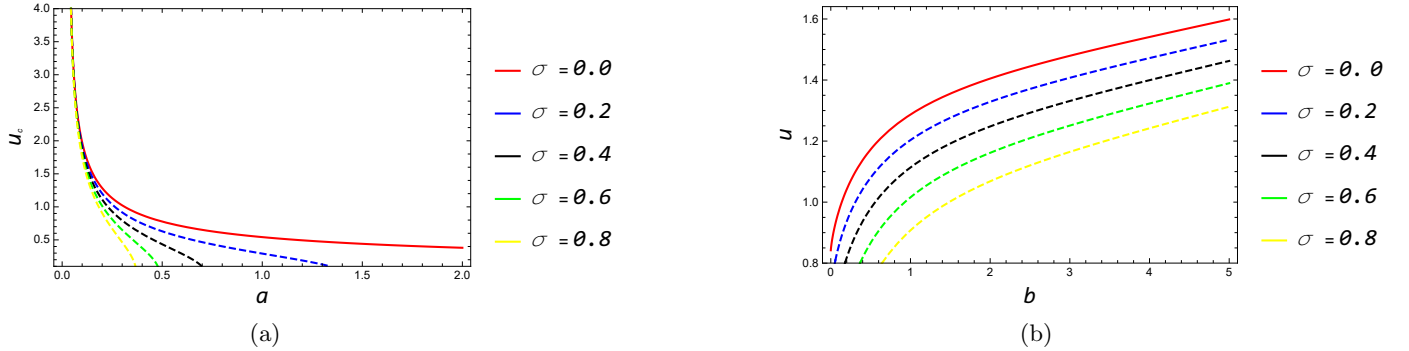


Figure 8: The impact parameter u_c as a function of a (Left panel) and b (Right panel) for the values of $\sigma = 0.0, 0.2, 0.4, 0.4, 0.6, 0.8$. Parameter $\sigma = \frac{\omega_p}{\omega_\infty}$ represents the ratio of plasma frequency and photon frequency.

We also can see that minimum impact parameter u_c in a homogeneous plasma medium is smaller than the vacuum case.

From the Eq.(40), the angle of deflection $\alpha(r_0)$ for the light ray coming from infinity to the Van der Waals BH in a homogeneous plasma medium can be written as

$$\alpha(r_0) = \phi(r_0) - \pi \quad (48)$$

where

$$\phi(r_0) = 2 \int_{r_0}^{\infty} \frac{d\phi}{dr} dr \quad (49)$$

$$\phi(r_0) = 2 \int_{r_0}^{\infty} \sqrt{\frac{G(r)}{R_p(r)K(r)}} dr \quad (50)$$

To calculate the angle of deflection in strong field limit, we apply an useful method developed by Bozza [5]. At first, we consider two new variables z and y as

$$y = 1 - \frac{r_0}{r} \quad (51)$$

Using the new variables, the total azimuthal angle $\phi(r_0)$ can be written as

$$\phi(r_0) = \int_0^1 F(y, r_0) dy = \int_0^1 \frac{2r_0}{\sqrt{G_p(y, r_0)}} dy \quad (52)$$

where

$$G_p(y, r_0) = \frac{R_p(z, r_0)K(z, r_0)}{G(z, r_0)} (1 - y)^4 \quad (53)$$

Above equation can be expanded as a power series of y in the following form

$$G_p(y, r_0) = \sum_{i=1}^{\infty} b_i(r_0) y^i \quad (54)$$

where $b_1(r), b_2(r)$ are given by [77]

$$b_1(r) = \frac{K_0 D_0 r_0}{G_0} \quad (55)$$

$$b_2(r) = \frac{H_0(r_0)r_0}{G_0} \left\{ D_0 \left[\left(D_0 - \frac{G'_0}{G_0} \right) r_0 - 3 \right] + \frac{r_0}{2} \left(\frac{K''_0}{K_0} - \frac{F''_0}{F_0} \right) \right\} \quad (56)$$

respectively

$$b_2(r_c) = \frac{K_c r_c^2}{2G_c} D'_c \quad (57)$$

where

$$D'_c = \frac{K''_0}{K_0} - \frac{F''_0}{F_0} \quad (58)$$

From the above discussion, we can obtain that the leading order of the divergence of $F(z, r_0)$ is y^{-1} , which shows that the integral $\phi(r_0)$ divergence logarithmically for $r_0 \rightarrow r_c$.

To solve, the integral in(52), it can be separated into a divergent $\phi_D(r_0)$ and a regular part $\phi_R(r_0)$ as

$$\phi(r_0) = \phi_D(r_0) + \phi_R(r_0) \quad (59)$$

where the divergent part is define as

$$\phi_D(r_0) = \int_0^1 g_D(y, r_0) dy \quad (60)$$

$$g_D(y, r_0) = \frac{2r_0}{\sqrt{b_1(r_0)y + b_2(r_0)y^2}} \quad (61)$$

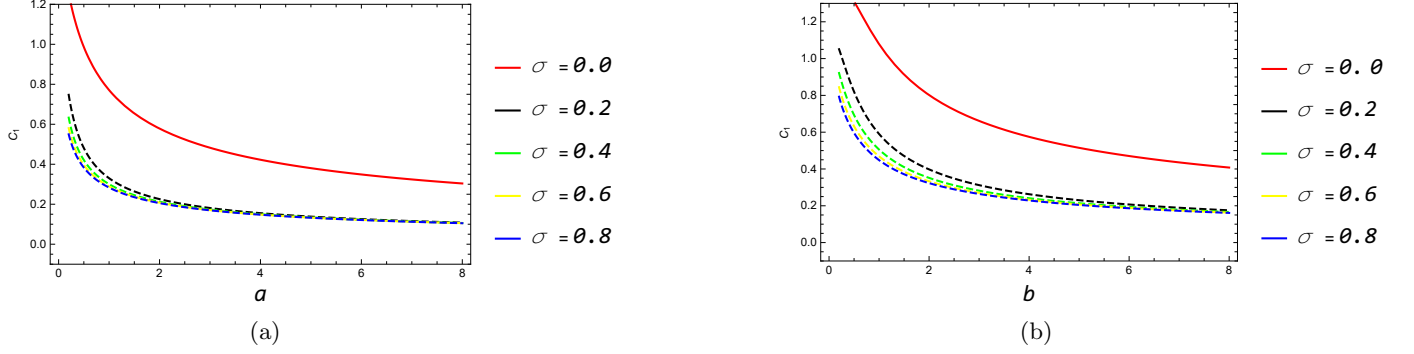


Figure 9: The strong deflection limit coefficient C_1 as a function of a (Left panel) and b (Right panel) for the values of $\sigma = 0.0, 0.2, 0.4, 0.4, 0.6, 0.8$. Parameter $\sigma = \frac{\omega_p}{\omega_\infty}$ represents the ratio of plasma frequency and photon frequency.

and integrating Eq.(60), we obtain

$$\phi_D(r_0) = \frac{4r_0}{\sqrt{b_2(r)}} \log \frac{\sqrt{b_2(r_0)} + \sqrt{b_1(r_0) + b_2(r_0)}}{\sqrt{b_1(r_0)}} \quad (62)$$

and the regular part is define as

$$\phi_R(r_0) = \int_0^1 g_R(y, r_0) dy \quad (63)$$

where

$$g_R(y, r_0) = g(y, r_0) - g_D(y, r_0) \quad (64)$$

The angle of deflection (for $r_0 \sim r_c$) can be represented as

$$\alpha(u) = -c_1 \log\left(\frac{u(r)}{u(r_c)} - 1\right) + c_2 + \mathcal{O}(u(r) - u(r_c)) \quad (65)$$

$$c_1 = \sqrt{\frac{2G_c}{K_m \left[\frac{(KW)_c''}{(KW)_c} - \frac{F_c''}{F_c} \right]}} \quad (66)$$

and

$$c_2 = -\pi + a_R + c_1 \log\left\{ r_c^2 \left[\frac{(KW)_c''}{(KW)_c} - \frac{F_c''}{F_c} \right] \right\} \quad (67)$$

$$a_R = \phi_R(r_c) = \int_0^1 g_R(y, r_c) dy.$$

Here, the subscript c indicates the value of the quantities at $r = r_c$

The strong deflection limit coefficients c_1 and c_2 with the parameter a (left panel) as well as the parameter b (right panel) are illustrated in Figs. 9 and 10. In Fig.9 we can see that for the fixed value of the parameter σ , the strong deflection limit coefficient c_1 decreases with the parameter a (left panel) as well as the parameter b (right panel). We also can see that the strong deflection limit coefficient c_1 in a homogeneous plasma medium is smaller than the vacuum case. In Fig.10 we can see that for the fixed value of the parameter σ , the strong deflection limit coefficient c_2 increases with the parameter a (left panel) while decreases with the parameter b (right panel). We also can see that the strong deflection limit coefficient c_2 in a homogeneous plasma medium is larger than the vacuum case. Using the strong deflection limit coefficients c_1 and c_2 , we can calculate the strong deflection angle $\alpha(u)$. For the different values of the parameter σ , behaviour the strong deflection angle $\alpha(u)$ with the parameter a (left panel) as well as the parameter b (right panel) is displayed in Fig.11. In this figure, it is easy to obtain that for the fixed value of the parameter σ , the strong deflection angle $\alpha(u)$ increases with the parameter a (left panel) as well as the parameter b (right panel). We also can see that the strong deflection angle $\alpha(u)$ in a homogeneous plasma medium is larger than that of vacuum medium.

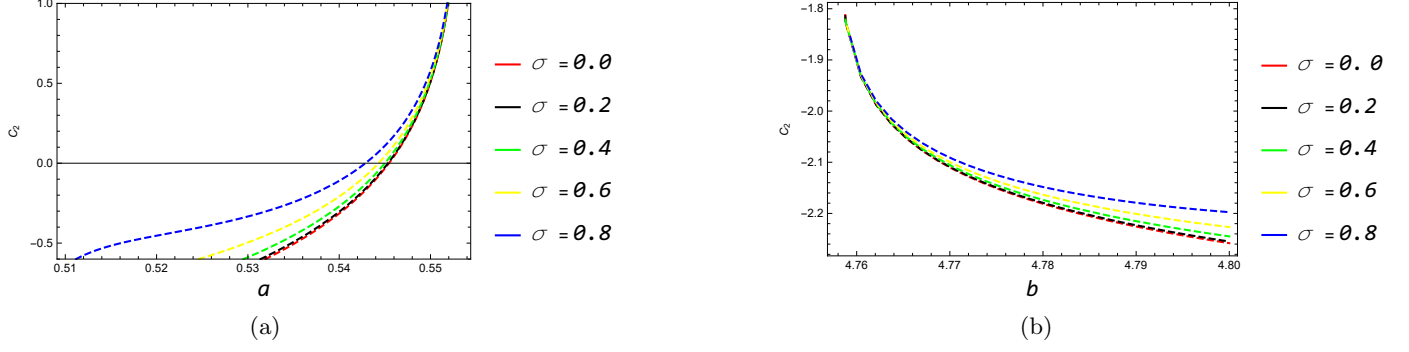


Figure 10: The strong deflection limit coefficient C_2 as a function of a (Left panel) and b (Right panel) for the values of $\sigma = 0.0, 0.2, 0.4, 0.4, 0.6, 0.8$. Parameter $\sigma = \frac{\omega_p}{\omega_\infty}$ represents the ratio of plasma frequency to the photon frequency.

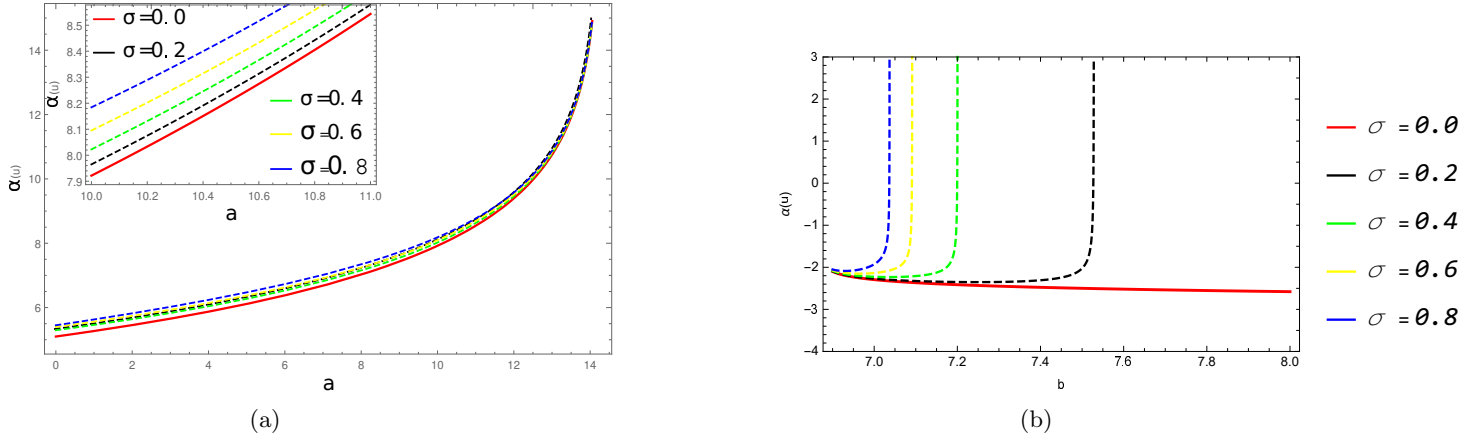


Figure 11: The strong deflection angle $\alpha(u)$ as a function of a (Left panel) and b (Right panel) for the values of $\sigma = 0.0, 0.2, 0.4, 0.4, 0.6, 0.8$. Parameter $\sigma = \frac{\omega_p}{\omega_\infty}$ represents the ratio of plasma frequency and photon frequency.

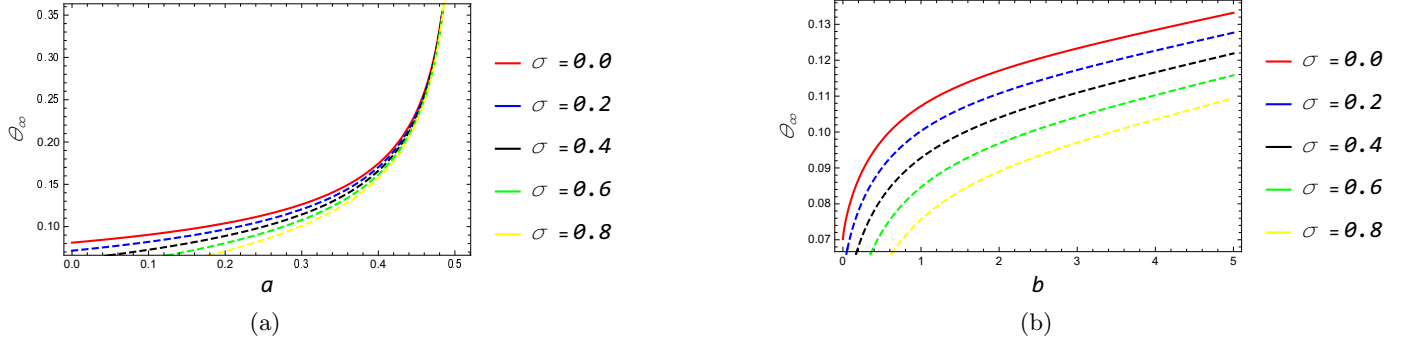


Figure 12: The angular position of image θ_∞ as a function of a (Left panel) and b (Right panel) for the values of $\sigma = 0.0, 0.2, 0.4, 0.6, 0.8$. Parameter $\sigma = \frac{\omega_p}{\omega_\infty}$ represents the ratio of plasma frequency and photon frequency.

6 Observables and Relativistic Images of Strong gravitational lensing

In this section, we study about the observables quantities of strong GL by Van der Waals BH with the effects of homogeneous plasma. Setting the BH at origin, the angle between the source and optical axis is denoted by β . Here, we are only interested in the case in which the lens, source and observer are almost alignment i.e. $\beta \simeq 0$. From the lens geometry in ref. [5, 79], the lens equation can be expressed in the strong field as

$$\beta = \left(\frac{D_{ls} - D_{ol}}{D_{ls}}\right)\theta - \alpha(\theta) \text{mod}(2\pi) \quad (68)$$

where D_{ls} and D_{ol} is the distance between lens and source and distance, and the distance between observer and lens respectively. The angle $\theta = \frac{u_c}{D_{ol}}$ represents the angular image position with respect to the optical axis.

Following Ref. [79–81], the angular position between the lens and the n^{th} relativistic image can be expressed as

$$\theta_n = \theta_n^0 \left(1 - \frac{u_c e_n (D_{ol} + D_{ls})}{\bar{a} D_{ol} D_{ls}}\right) \quad (69)$$

where

$$\theta_n^0 = \frac{u_c}{D_{ol}} (1 + e_n), \quad (70)$$

and

$$e_n = e^{-\frac{c_2 + |\beta| - 2n\pi}{c_1}} \quad (71)$$

As in Ref. [79–81], we consider a simple case in which only the outer most image i.e., the first image θ_1 is treated as a single image and all the others images are packed together at θ_∞ . With the help of equations (69) and (70), one can obtain the angular position of set of images θ_∞ related to the minimum impact parameter u_c as

$$\theta_\infty = \frac{u_c}{D_{ol}} \quad (72)$$

The observable quantity S , the angular image separation between the first image θ_1 and the others images can be obtained as

$$s = \theta_1 - \theta_\infty = \theta_\infty e^{-\frac{c_2 - 2n\pi}{c_1}} \quad (73)$$

and the observable quantity r_{mag} , the ratio of the flux between the first image θ_1 and the others images as

$$r_{mag} = \exp\left(\frac{2\pi}{c_1}\right) \quad (74)$$

If the observables quantities $\theta_\infty, S, r_{mag}$ are available from the observations, the strong deflection limit coefficients c_1, c_2 and the impact parameter u_c can be calculate easily and then compared to theoretical values.

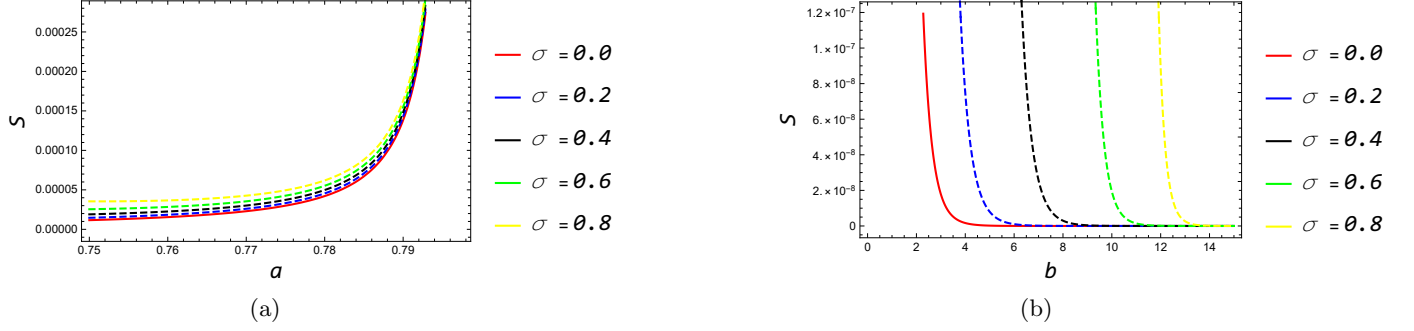


Figure 13: The angular separation of the images s as a function of a (Left panel) and b (Right panel) for the values of $\sigma = 0.0, 0.2, 0.4, 0.4, 0.6, 0.8$. Parameter $\sigma = \frac{\omega_p}{\omega_\infty}$ represents the ratio of plasma frequency and photon frequency.

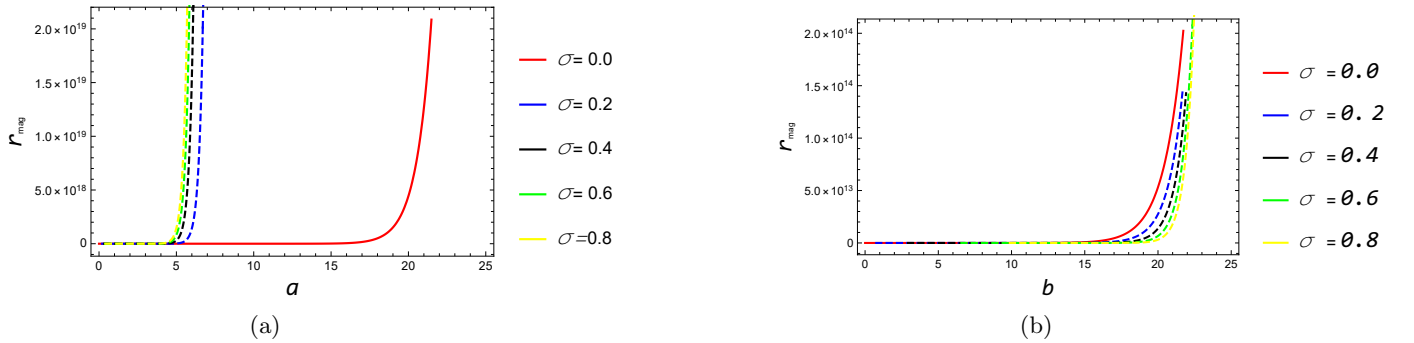


Figure 14: The relative magnification r_{mag} as a function of a (Left panel) and b (Right panel) for the values of $\sigma = 0.0, 0.2, 0.4, 0.4, 0.6, 0.8$. Parameter $\sigma = \frac{\omega_p}{\omega_\infty}$ represents the ratio of plasma frequency and photon frequency.

We plot the strong observable quantities θ_∞ , S and r_{mag} in a realistic scenario of the BH, such as $SgrA^*$ having mass $M = 6.5 \times 10^6 M_\odot$ and $D_{ol} = 16.8 Mpc$ [82] are displayed in Figs.(12),(13),and (14) by assuming $D_{ls} = 1 kpc$. We can see that for the fixed value of the parameter σ , the strong observable quantities θ_∞ and r_{mag} increases with the parameter a (left panel) as well as the parameter b (right panel), respectively in Fig.13 and Fig.14. We also can see that strong observable quantity θ_∞ in a homogeneous plasma medium is smaller than that of vacuum medium with respect to the parameter a as well as the parameter b . But the strong observable quantities r_{mag} in a homogeneous plasma medium is smaller than the vacuum medium with respect to the parameter a while larger than the vacuum medium with respect to the parameter b . In Fig.13, we can see that with the fixed value of the parameter σ , the angular separation S increases with the parameter a (left panel) and decreases with the parameter b (right panel). In this figure, we can also see that the angular separation S in a homogeneous plasma medium is smaller than that of a vacuum medium with respect to the parameter a as well as the parameter b .

7 Discussions and Conclusions

In this work, we have discussed the Shadows and strong gravitational lensing (GL) by Van der Waals BH in the presence of a homogeneous plasma medium. At first, we analyzed the horizon structure of the Van der Waals BH. Next, we have analytically calculated the first order null geodesic equation by the Hamiltonian-Jacobi separation method. As an application of null geodesic equations, one can determine BH shape as well as shadow shape. With the help of these geodesics equations, we calculate and discuss the shadows of the Van der Waals BH in the absence of plasma medium as well as the presence of plasma medium, respectively. In this work, we graphically calculate the radius of the photon sphere with the different values of parameters a , b and with the different values of parameters σ , respectively. We observe that for the fixed value of the parameter a , radius of shadows of the BH decreases while the parameter b increases in the absence of a plasma medium. In the presence of a homogeneous plasma medium, we have calculated the circular radius of the photon sphere for the different values of the parameter σ (the Parameter $\sigma = \frac{\omega_p}{\omega_\infty}$ represents the ratio of plasma frequency and photon frequency) graphically.

We have also seen that the radius of shadows of the BH in a homogeneous plasma medium decreases while the parameter σ increases and the radius of shadows in a homogeneous plasma medium is larger than the vacuum medium. Next, we studied the strong GL with the effects of a homogeneous plasma medium. We have studied the effects of VdW parameters a , b and the parameter σ (the ratio of plasma frequency to the photon frequency) on the strong deflection angle $\alpha(u)$ and strong lensing observables $\theta_\infty, S, r_{mag}$ in a homogeneous plasma medium and compared to the vacuum medium. We find that for the fixed value of σ , the strong deflection angle increases with the parameters a as well as b . We also see that the deflection angle in the strong field with the presence of a homogeneous plasma medium is larger than the vacuum cases. We have studied the observables quantities angular position θ_∞ , separation S and magnification r_{mag} by taking the example of super massive BH $SgrA^*$ in the strong field limit with the effects of homogeneous plasma. We have seen that strong observable quantities θ_∞ and S in a homogeneous plasma medium are smaller than that of a vacuum medium with respect to the parameter a as well as the parameter b and the strong observable quantities r_{mag} in a homogeneous plasma medium is smaller than the vacuum medium with respect to the parameter a while larger than the vacuum medium with respect to the parameter b .

Acknowledgement: NUM is thankful to CSIR, Govt. of India for providing Senior Research Fellowship (No. 08/003(0141))/2020-EMR-I).

References

- [1] C. Darwin, Proc. R. Soc. Lond. **249**, 180 (1959).
- [2] K. Virbhadra and G. F. Ellis, Phys. Rev. D **62**, 084003 (2000).
- [3] S. Frittelli, T. P. Kiling and E. T. Newman, Phys. Rev. D **61**, 064021 (2000).
- [4] V. Bozza, S. Caozziello, G. Iovane and G. Scapetta, Gen. Relativ. Gravit. **33**, 1535 (2001).

- [5] V. Bozza, Phys. Rev. D **66**, 103001 (2002).
- [6] J. P. Luminet, Astron. Astrophys. **75** , 228-235(1979).
- [7] H. C. Ohanian, Am. J. Phys. **55**, 428 (1987).
- [8] R. J. Nemiroff, Am. J. Phys. **61**, 619 (1993).
- [9] M. Sharif and S. Iftikhar Astrophysics and Space Science, **361**, 36 (2016) .
- [10] N. U. Molla and U. Debnath, Int.J.Mod.Phys.A **36** , 27, 2150210(2021).
- [11] K. Akiyama et al. (Event Horizon Telescope Collaboration), Astrophys. J. **875**, L1 (2019).
- [12] K. Akiyama et al. Astrophys. J. **875**, L2 (2019).
- [13] K. Akiyama et al. , Astrophys. J. **875**, L3 (2019).
- [14] K. Akiyama et al. , Astrophys. J. **875**, L4 (2019).
- [15] K. Akiyama et al. , Astrophys. J. **875**, L5 (2019).
- [16] K. Akiyama et al. , Astrophys. J. **875**, L6 (2019).
- [17] H. Falcke, F. Melia, and E. Agol, Astrophys. J. Lett. **528**, L13 (2000).
- [18] L. Amarilla and E. F. Eiroa, Phys. Rev. D **85**, 064019(2012).
- [19] T. Johannsen, Astrophys. J. **777**, 170 (2013).
- [20] A. de Vries, Classical Quantum Gravity **17**, 123 (2000).
- [21] L. Amarilla, E. F. Eiroa and G. Giribet, Phys. Rev. D **81**, 124045 (2010).
- [22] L. Amarilla and E. F. Eiroa, Phys. Rev. D **87**, 044057 (2013).
- [23] A. Yumoto, D. Nitta, T. Chiba and N. Sugiyama, Phys. Rev. D **86**, 103001 (2012).
- [24] A. Abdujabbarov, M. Amir, B. Ahmedov and S. G. Ghosh, Phys. Rev. D **93**, 104004 (2016).
- [25] M. Amir and S. G. Ghosh, Phys. Rev. D **94**, 024054 (2016).
- [26] N. Tsukamoto, Z. Li and C. Bambi, J. Cosmol. Astropart. Phys. **1406**, 043 (2014).
- [27] K. Hioki and K. i. Maeda, Phys. Rev. D **80**, 024042 (2009).
- [28] C. Bambi and N. Yoshida, Class. Quant. Grav. **27**, 205006 (2010).
- [29] C. Goddi et al., Int. J. Mod. Phys. D **26**, 1730001 (2016).
- [30] R. Takahashi, Publ. Astron. Soc. Jap. **57**, 273 (2005).
- [31] S. W. Wei and Y. X. Liu, J. Cosmol. Astropart. Phys. **11**, 063 (2013).
- [32] A. Abdujabbarov, F. Atamurotov, Y. Kucukakca, B. Ahmedov, and U. Camci, Astrophys. Space Sci. **344**, 429 (2013).
- [33] L. Amarilla and E. F. Eiroa, Phys. Rev. D **85**, 064019 (2012).
- [34] C. Bambi and K. Freese, Phys. Rev. D **79**, 043002 (2009).
- [35] F. Atamurotov, A. Abdujabbarov, and B. Ahmedov, Phys. Rev. D **88**, 064004 (2013).
- [36] M. Wang, S. Chen and J. Jing, J. Cosmol. Astropart. Phys. **1710**, 051 (2017).
- [37] J. Schee and Z. Stuchlik, Int. J. Mod. Phys. D **18**, 983 (2009).

- [38] A. Grenzebach, V. Perlick, and C. Lämmerzahl, Phys. Rev. D **89**, 124004 (2014).
- [39] B. P. Singh, Annals Phys. **441**, 168892 (2022)
- [40] R. Kumar, B. P. Singh and S. G. Ghosh, Annals Phys. **420**, 168252 (2020).
- [41] R. Kumar, B. P. Singh, M. S. Ali and S. G. Ghosh, Phys. Dark Univ. **34**, 100881 (2021).
- [42] R. Kumar and S. G. Ghosh, JCAP **07**, 053 (2020).
- [43] B. Narzilloev, I. Hussain, A. Abdujabbarov and B. Ahmedov, Eur. Phys. J. Plus **137**, no.5, 645 (2022).
- [44] S. W. Wei, Y. C. Zou, Y. X. Liu and R. B. Mann, JCAP **08**, 030 (2019).
- [45] U. Papnoi and F. Atamurotov, Phys. Dark Univ. **35**, 100916 (2022).
- [46] F. Atamurotov, U. Papnoi and K. Jusufi, Class. Quant. Grav. **39**, no.2, 025014 (2022).
- [47] A. Chamblin, R. Emparan, C.V. Johnson and R.C. Myers, Phys. Rev. D **60**, 064018 (1999) .
- [48] M. Cvetič and S.S. Gubser, JHEP **04**, 024,(1999).
- [49] C. Niu, Y. Tian and X.-N. Wu, Phys. Rev. D **85** 024017(2012).
- [50] D. Kubiznak and R.B. Mann, JHEP **07**, 033 (2012) .
- [51] S. Gunasekaran, R. B. Mann, and D. Kubiznak, JHEP **1211**, 110(2012) .
- [52] J.D.E. Creighton and R.B. Mann, Phys. Rev. D **52** 4569 (1995).
- [53] M.M. Caldarelli, G. Cognola and D. Klemm, Class. Quant. Grav. **17**, 399 (2000) .
- [54] A. Rajagopal, D. Kubiznak and R. B. Mann, Phys. Lett. B **737**, 277 (2014).
- [55] T. Roy and U. Debnath Int.J.Mod.Phys.A **36** , 17, 2150114(2021).
- [56] V. Perlick, O. Yu. Tsupko, G. S. Bisnovatyi-Kogan, Phys.Rev.D **92** ,10, 104031(2015) . Published in: Phys.Rev.D **92** , 10, 104031 (2015).
- [57] N. Tsukamoto, Phys.Rev.D **102** , 10, 104029 (2020).
- [58] J. L. Synge, Relativity: the General Theory (North-Holland Publishing Company, Amsterdam, 1960).
- [59] V. Perlick, Ray Optics, Fermats Principle, and Applications to General Relativity (Springer-Verlag, Berlin, 2000).
- [60] G. S. Bisnovatyi-Kogan and O. Y. Tsupko, Universe **3** , no.3, 57 (2017).
- [61] A. Abdujabbarov, B. Toshmatov, Z. Stuchlk and B. Ahmedov, Int. J. Mod. Phys. D **26** ,no.06, 1750051(2016) .
- [62] V. Perlick and O. Y. Tsupko, Phys. Rev. D **95** ,no.10, 104003(2017).
- [63] A. Abdujabbarov, B. Juraev, B. Ahmedov and Z. Stuchlk, Astrophys. Space Sci. **361** ,no.7, 226 (2016) .
- [64] Y. Huang, Y. P. Dong and D. J. Liu, Int. J. Mod. Phys. D **27** , no.12, 1850114 (2018).
- [65] C.-Q. Liu, C.-K. Ding, J.-L. Jing, Chin.Phys.Lett. **34** , 9, 090401(2017).
- [66] G. Bisnovatyi-Kogan and O. Tsupko, Grav. Cosmol. **15** , 20-27 (2009).
- [67] G. Bisnovatyi-Kogan and O. Tsupko, Mon. Not. Roy. Astron. Soc. **404** , 1790-1800 (2010).
- [68] V. Morozova, B. Ahmedov, and A. Tursunov, Astrophys. Space Sci. **346**, 513 (2013).
- [69] X. Er and S. Mao, Mon. Not. Roy. Astron. Soc. **437** , no.3, 2180-2186 (2014).

- [70] F. Atamurotov and B. Ahmedov, Phys. Rev. D **92** , 084005 (2015).
- [71] A. Rogers, Mon. Not. Roy. Astron. Soc. **451**, 4536 (2015).
- [72] V. Perlick, O. Y. Tsupko and G. S. Bisnovatyi-Kogan, Phys. Rev. D **92** , no.10, 104031(2015).
- [73] O. Y. Tsupko and G. S. Bisnovatyi-Kogan, Phys. Rev. D **87** ,no.12, 124009 (2013) .
- [74] R. Kulsrud and A. Loeb, Phys. Rev. D **45** , 525-531(1992).
- [75] X.-H. Jin, Y.-X. Gao, D.-J. Liu, Int.J.Mod.Phys.D **29** , 09, 2050065 (2020).
- [76] N. Tsukamoto, Phys. Rev. D **94** , no.12, 124001(2016) .
- [77] N. Tsukamoto , Phys.Rev.D **95** , 6, 064035(2017) .
- [78] V. Perlick, O. Y. Tsupko and G. S. Bisnovatyi-Kogan, Phys. Rev. D **92** , no.10, 104031,(2015).
- [79] V. Bozza, Phys. Rev. D **67**, 103006 (2003).
- [80] V. Bozza, F. De Luca, G. Scarpetta, M. Sereno, Phys. Rev. D **72**, 083003 (2005);
- [81] V. Bozza, F. De Luca, G.Scarpetta, Phys. Rev. D **74**, 063001(2006).
- [82] I. Banerjee, S.Sau, S. SenGupta, 2022, e-Print: 2207.06034 [gr-qc]